Check for updates

A cradle to cradle approach towards remediation of uranium from water using carbonized arecanut husk fiber†

V. Dhanya and N. Rajesh [ID] *

Sustainable materials for remediation of pollutants from water is the need of the hour. In this study two carbonaceous adsorbents prepared through hydrothermal carbonisation and pyrolysis from arecanut husk fiber, an agricultural waste material were used for the adsorption of uranium from water. Batch adsorption data as interpreted using the Langmuir model showed adsorption capacities of 250 mg g^{-1} and 200 mg g^{-1} respectively at pH 6 for the hydrochar (AHFC) and the pyrochar (AHFT) exceeding that reported for most of the unmodified biochars. The adsorption followed pseudo-second order kinetics and was exothermic in nature. The high selectivity and excellent removal efficiencies on application to environmental ground water samples and good regeneration capacity make these sorbents promising eco-friendly materials for uranium remediation from water.

1. Introduction

Radioactivity and chemical toxicity of uranium renders it a global health hazard when present in ground water. Geochemical reactions, mining, natural disposition from minerals, uranium ore processing and spent fuel disposal are some of the ways by which the metal enters the aquatic environment.[1] The WHO has set the permissible limit for uranium in ground water to a maximum of 30 ppb. However, many countries including India have reported ground water contamination by uranium.[2] A major source of uranium contamination in ground water includes geogenic, leaching from aquifers containing uranium minerals and other anthropogenic activities such as the use of phosphate and nitrate containing fertilizers for agriculture. On oxidation, uranium transforms to uranyl ions (UO_2^{2+}) that easily dissolve in water where they get stabilized in the presence of common anions like carbonate, hydroxide and phosphate present in water.[3] Therefore, it is very important to develop purification technologies for safe drinking water as per the sustainable development goals (UNSDG Goal 6) of the United Nations.

Many techniques are reported for remediation of uranium from aqueous systems. A recent review tabulated various conventional technologies, their advantages, limitations and also brought out the recent developments of efficient and eco-friendly bio-sorbents for uranium remediation.[4] A few of the

Department of Chemistry, Birla Institute of Technology and Science, Pilani, Hyderabad Campus, Jawahar Nagar, Hyderabad 500078, India. E-mail: nrajesh@hyderabad. bits-pilani.ac.in

† Electronic supplementary information (ESI) available. See DOI: https://doi.org/10.1039/d2ra08333g

technologies demonstrated include reverse osmosis, ultra/nano filtration, ion-exchange, precipitation and setting up of a permeable reactive barrier (PRB) using zerovalent iron.[5–7] However, adsorption based techniques are known to be the most effective and eco-friendly option for uranium removal from aqueous systems. Several materials have been reported as good adsorbents for uranium that include activated mesoporous carbon, carbon nanofiber, graphene and their functionalized counterparts, covalent organic framework, metal organic framework, nano-silica, nano-TiO$_2$, biochar, polymer resins and microorganism based materials.[8–19] Carbon materials are extremely promising because of chemical stability, easy operation and recyclability.[20]

Currently a lot of focus is given to the development of adsorbents from waste materials by suitable modifications, adhering to the "waste to wealth" principle.[21–23] Biomass has been identified as a green resource for the synthesis of char based adsorbents for decontamination of water from phosphates,[24] organic pollutants[25] and many heavy metal ions.[26] Biochar is produced by the thermal degradation of biomass under oxygen limited conditions. Carbon-richness, large surface area and abundant functional groups enable biochar to be effectively used in carbon sequestration, environmental remediation and wastewater treatment. Biochar production from biowaste is considered as an appropriate technology to produce efficient adsorbents having high surface area and enriched functional groups at low cost.[27,28] Low cost biochars have been prepared from various sources such as rice straw, pig manure, cow dung, plant twigs stem, leaves and root, fruits and their peels and shells of nuts.[29] These biomass materials are either used directly in powdered form or after carbonization through pyrolysis and hydrothermal processes and also as

functionalized carbonaceous materials. As hydrothermal method uses water as a reagent for hydrolysis of organic compounds in biomass, it's carbon foot print is much low compared to the biochar prepared through pyrolysis route.[30]

Among the naturally available agricultural waste materials, arecanut husk fiber (AHF) has been used as a biomass resource for preparation of biochar for environmental applications. Around 1.8 million tons of arecanut per year is produced globally and 54% of this is from India alone. Most of the husk fiber waste produced is discarded by burning as it does not decompose easily adding to air pollution. Although several studies are reported[31] on the use of areca plant materials for waste water treatment, not much has been explored on its applicability for uranium remediation. In this work, areca-nut husk fibre in its raw powdered form (AHF), biochars produced through hydrothermal route (AHFC) and through pyrolysis (AHFT) in low oxygen atmosphere are compared for adsorptive removal of uranium from contaminated ground water. The synthesis, characterization, isotherms, kinetic and mechanistic interaction of dissolved uranium ions with the adsorbents, selectivity, recyclability and application to natural and doped ground water samples are discussed.

2. Experimental

2.1. Materials and methods

Arecanut husk was sourced from agricultural farms of Malappuram district in Kerala, India. Orthophosphoric acid, HNO_3 and NaOH and ammonium dihydrogen phosphate were obtained from SRL Chemicals, India. For all dilutions, Millipore water was used. Stock solution of uranium (2000 mg L^{-1}) was prepared using $UO_2(NO_3)_2 \cdot 6H_2O$ purchased from SRL Chemicals, India.

250 g of ammonium dihydrogen phosphate was dissolved in 500 mL Milli-Q water followed by addition of 60 mL orthophosphoric acid and made up to 1000 mL for preparing fluorescence enhancing buffer (pH 2) used in spectrofluorimetric determination of uranium.

2.2. Quantification of uranium by spectrofluorimetry

Quantification of uranium in aqueous solutions was done using a Spectramax iD3 spectrofluorimeter. An excitation wavelength of 300 nm was chosen for this work due to its high intensity and relatively lesser quenching effects even though the absorption spectrum of uranium spreads from 200 to 420 nm. The fluorescence measurements were done at 516 nm, it being the most intense peak among the three distinct peaks at 490 nm, 516 nm and 540 nm characteristic of the uranium fluorescence spectrum. A 40% (v/v) of the fluorescence enhancing buffer was maintained in all solutions equilibrated to 20 °C prior to fluorescence intensity measurement.

2.3. Synthesis of adsorbents

Hydro thermal carbonisation and pyrolysis were carried out in an autoclave using an oven (Bio-Technics India) and a tubular furnace with N_2 flow (Nabertherm) respectively. Arecanut husk fiber (AHF) was cleaned with distilled water, dried in a hot air oven for 24 hours and powdered. The powder was sieved to get uniform size particles. The powder and deionized water were mixed in the ratio 1 g : 10 mL and sonicated for 15 minutes. This mixture was then added to Teflon lined autoclave and hydrothermal carbonization was carried out by heating at 180 °C for 24 hours in an oven. The hydrochar (AHFC) thus obtained was cooled, washed five times with 10% NaOH and deionized water, filtered using Whatman 40 filter paper and dried. Dried hydrochar was finely powdered using mortar and pestle and weighed. The yield obtained was noted to be 50%. The powdered arecanut husk fiber was also pyrolysed in a tubular furnace at 300 °C for 2 hours under N_2 atmosphere to get the carbonized form (AHFT). The carbon obtained was washed with deionized water, dried and finely powdered. Batch adsorption studies were carried out with both the adsorbents.

2.4. Characterization of adsorbents

A Shimadzu IRAffinity-IS model spectrometer was used for recording the FT-IR spectra of adsorbents in the range 400–4000 cm^{-1}. Raman spectra of the adsorbents were recorded using UniRAM-3300 Micro Raman Mapping Spectrophotometer for which the excitation source was a solid state laser at 532 nm. Malvern Zetasizer Nano ZS was used to measure the zeta potential of the adsorbents at varying pH values. Surface morphology studies and elemental mapping of the adsorbents were conducted using Apreo LoVac, FEI scanning electron microscope coupled with an EDX analysis system (Oxford X-Max). The oxidation states of uranium on the sorbents were identified with the help of K-alpha, Thermo Fisher Scientific XPS instrument with aluminium monochromator. A Quantachrome, St 2 on NOVA touch 4LX instrument was used to measure the surface area, pore size and pore volume of the adsorbents using Brunauer–Emmett–Teller method. The thermal stability of the adsorbents was analysed using a Shimadzu (DTG-60) model thermal analyser in the temperature range of 30–800 °C at a heating rate of 10 °C min^{-1} in a nitrogen atmosphere.

2.5. Sorption experiments

A stock solution of 2000 mg L^{-1} of uranium was prepared by dissolving uranyl nitrate ($UO_2(NO_3)_2 \cdot 6H_2O$) in Millipore water. Isotherm study at room temperature was conducted with solutions of concentrations 2, 5, 10, 20, 50, 100, 200, 300, 350, 400, 450 and 500 mg L^{-1}. An initial concentration of 10 mg L^{-1} of uranium was used for the optimisation of the pH of adsorption at 6 by adding 0.1 M NaOH and 0.1 M HNO_3 solutions. Equilibrium was attained by agitating 10 mL of uranium solutions of varying concentrations with 10 mg of sorbents for 1 hour at 30 °C and 120 rpm in an orbital incubator shaker (Bio Technics, India). The solutions were then filtered using (Whatman 45) filter paper. Any precipitation at pH 6 and the adsorption on to the filter paper were checked using uranium solution without the adsorbents in the control experiments and were found to be minimal. A spectrofluorimeter calibrated using a series of standards containing 0.1, 0.5, 1.0, 5.0 mg L^{-1} uranium was used

for the determination of concentration of uranium before and after adsorption maintaining 10 mL fluorescence enhancing buffer in 25 mL solution.

The percentage removal of uranium was calculated using the eqn (1)

$$U(removal)\% = \frac{C_0 - C_f}{C_0} \times 100 \qquad (1)$$

The equilibrium adsorption capacities (q_e) were calculated using eqn (2)

$$q_e = \frac{(C_0 - C_e)V}{m} \qquad (2)$$

where C_o, C_f and C_e are the initial, final and equilibrium concentrations (mg L^{-1}) of U(VI) respectively, V is the volume of solution (L) and m is the mass of adsorbent (g) used.

The experimental data was fitted with Langmuir and Freundlich isotherm models.

3. Results and discussion

3.1. Preparation of adsorbents

The raw arecanut husk fiber was washed, dried and powdered and this powder was used for adsorption of uranium which showed 70% removal efficiency from 10 ppm uranium solution at pH 6 with an adsorbent dosage of 10 mg. Hydrothermal carbonization was performed separately by mixing the powder with water as well as with acetic acid. Interestingly the adsorption efficiency remained almost the same (90%) for the hydrochars obtained by both ways and it was decided to use water only as the medium. Washing of the hydrochar with 10% NaOH solution and subsequently with deionized water was done till the filtrate turned colorless. The temperature and time for pyrolysis were optimized to be 300 °C and 2 hours checking the completion of carbonization at varying conditions for the preparation of the pyrochar. The pH of water after adding both the adsorbents was found neutral and were then used in powdered form for batch adsorption of uranium. The trial

adsorption study with the hydrochar and pyrochar showed 85% and 87% removal efficiency from 10 ppm solution of uranium which was much higher than that of AHF. Hence further adsorption studies were conducted with AHFC and AHFT.

3.2. Characterization of the adsorbent

3.2.1. SEM and EDX analysis.
The morphologies and elemental distribution of the adsorbents were interpreted using SEM and EDAX data (Fig. 1, 2 and 3). The SEM images clearly depicted the elongated, cylindrical, fibrous and porous structure of AHF, AHFC and AHFT. The surface of AHF was smoother whereas some fissures were observed on the surface of AHFC and AHFT which could be due to the disintegration of hemicelluloses and cellulose from the lignocellulosic matrix on hydrothermal carbonization and pyrolysis.[32] The porosity increased in AHFC and AHFT compared to the raw fiber and the pores were clearly visible in both the hydrochar and the pyrochar with the appearance of droplet like depositions. The SEM images of adsorbents after adsorption (AHFCU and AHFTU) showed the filling of the pores with the metal ion. The elemental composition before and after adsorption was determined using EDX data (Table 1) which revealed a significant increase in the weight percentages of carbon in both the adsorbents as compared to the raw fiber. Elemental mapping depicted the presence of uranium on the surface of the adsorbents.

3.2.2. FTIR and Raman spectra analysis.
FTIR spectra of AHF, AHFC and AHFT were studied for a comparison of the functional groups present in them (Fig. 4a). The raw husk fiber gave a strong band at 3443 cm^{-1} corresponding to pure lignin O–H which was not found in AHFC and AHFT indicating the removal of lignin during the carbonization and the treatment with NaOH solution.[33] The peak in AHF at 1653 cm^{-1} corresponds to carboxyl groups conjugated with aromatic rings and the one at 1421 cm^{-1} is due to methoxyl group both of which were missing in AHFC and AHFT. Prominent changes in the chemistry of the material after the carbonization process could be inferred from these results which resulted in improved
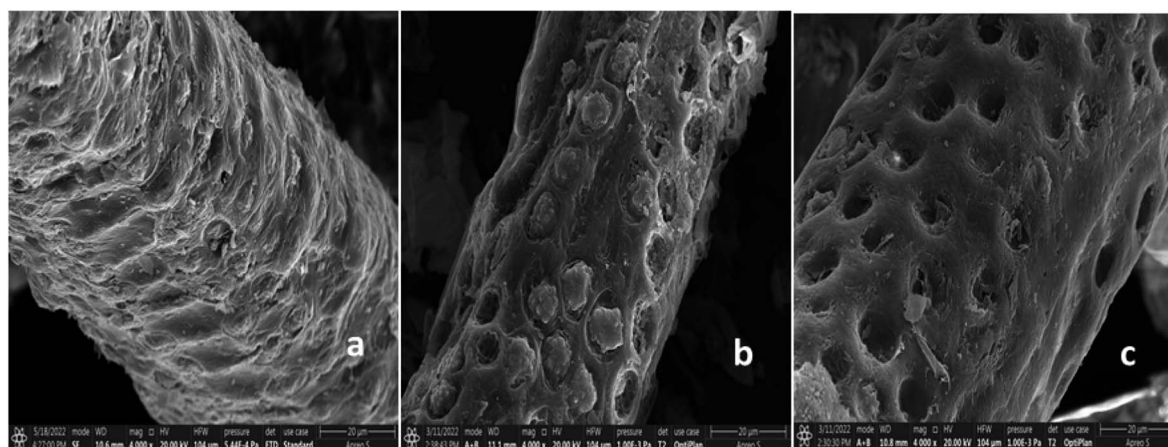

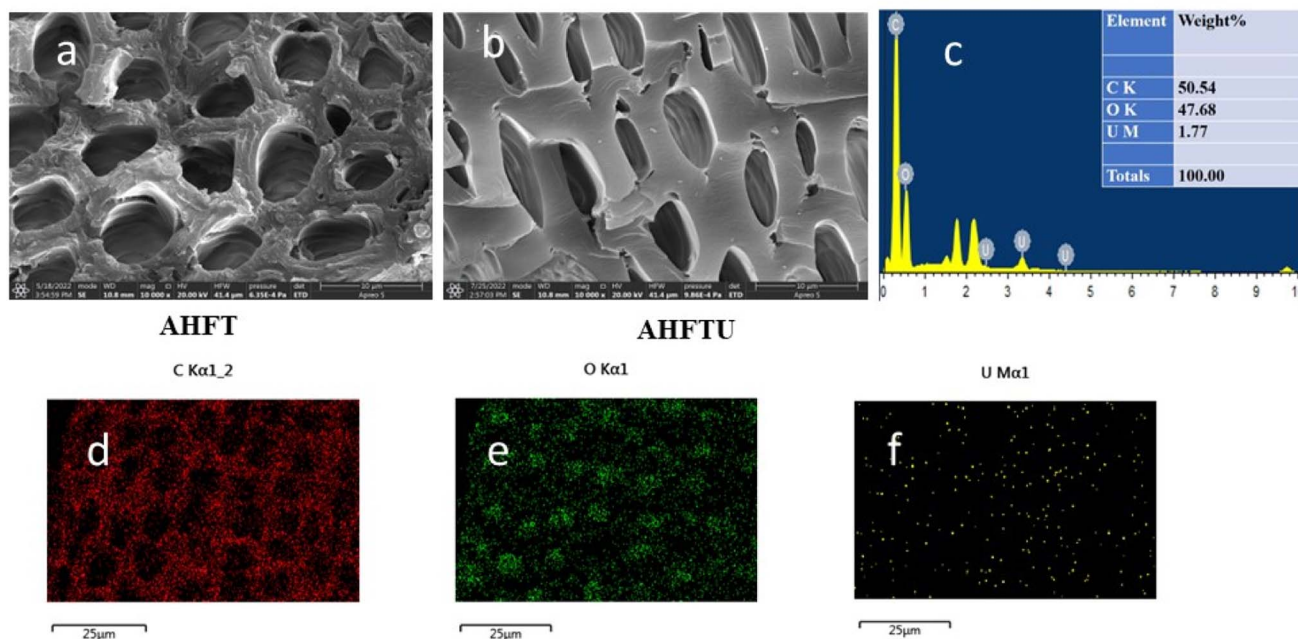Fig. 1 SEM images of (a) AHF, (b) AHFC and (c) AHFT.

Element	Weight%
C K	50.54
O K	47.68
U M	1.77
Totals	100.00

Fig. 2 SEM images of (a) AHFT (b) AHFTU (c) EDAX spectrum of AHFTU, elemental mapping images depicting distribution of (d) carbon, (e) oxygen and (f) uranium.
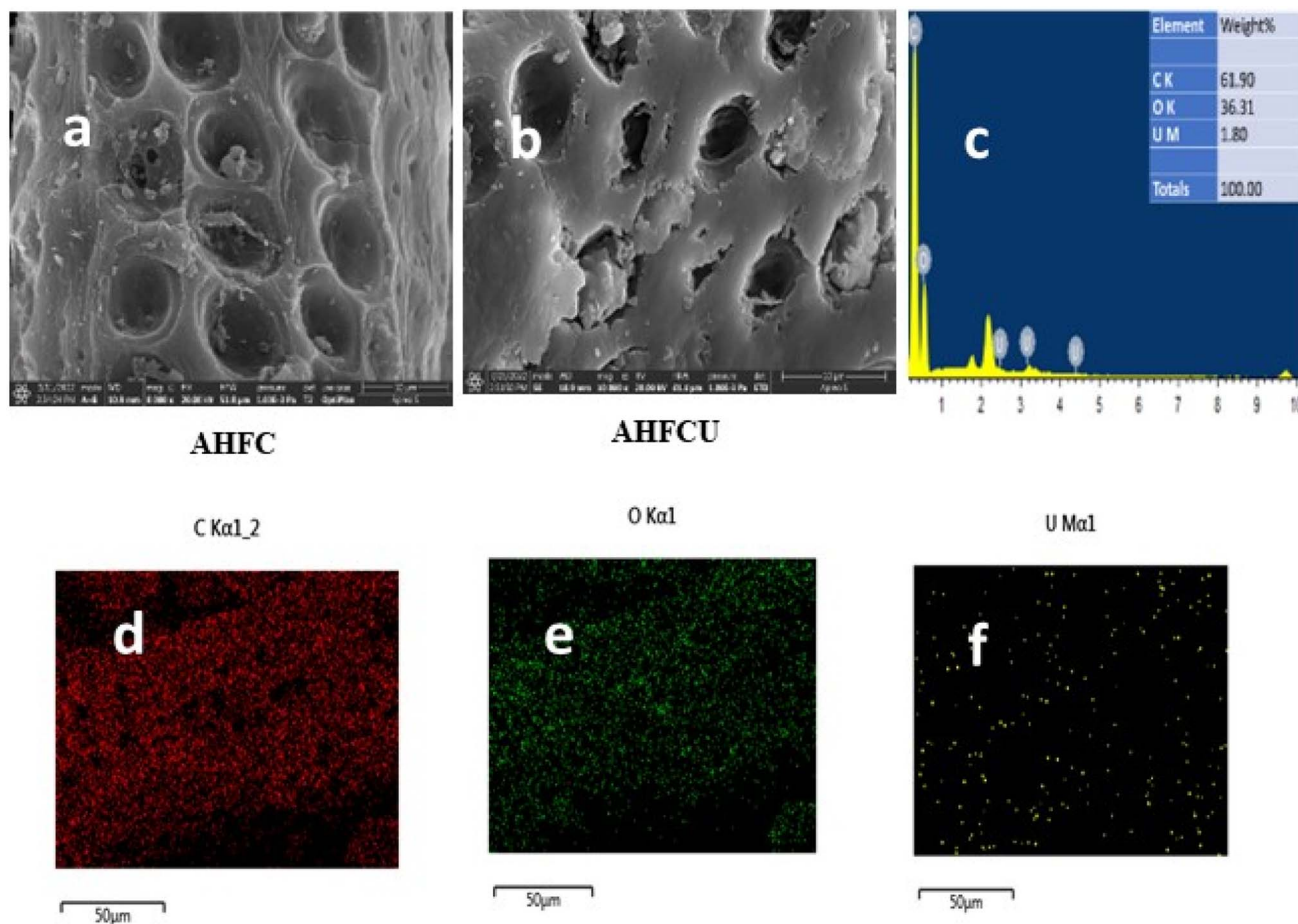

Element	Weight%
C K	61.90
O K	36.31
U M	1.80
Totals	100.00

Fig. 3 SEM images of (a) AHFC (b) AHFCU (c) EDAX spectrum of AHFCU, elemental mapping images depicting distribution of (d) carbon, (e) oxygen and (f) uranium.

Table 1 Elemental composition of AHFU, AHFCU and AHFTU

Material	Weight (%) [EDAX analysis]		
	C	O	U
AHFU	50.73	48.95	0.32
AHFCU	61.90	36.30	1.80
AHFTU	50.54	47.68	1.77

adsorption efficiency. New peaks at 1770 cm^{-1} and 1736 cm^{-1} respectively in AHFC and AHFT indicates the presence of C=O group. The peaks at 661 cm^{-1} and 671 cm^{-1} in AHFCU and AHFTU indicated the presence uranium bonded to oxygen on the adsorbents (Fig. 4b).[34] The Raman spectra of the adsorbents were analyzed to understand the nature of the carbon skeleton in the adsorbents (Fig. 5). The appearance of an intense G band in AHFC and AHFT indicated the presence of sp^2 carbon in graphitic layered structure.[35] Intensity of the G band for AHFT was slightly less compared to that of AHFC indicating a change in structure of the carbons obtained through hydrothermal and pyrolytic modes of synthesis. A distinct D band was observed in the case of AHFCU which was absent in AHFC showing the introduction of defects in the carbon skeleton after adsorption. D band was observed in both AHFT and AHFTU as well but with lesser intensities and with no significant change before and after adsorption. This striking difference in appearance of D bands correlates with the better adsorption capacity shown by AHFC in comparison with AHFT.

3.2.3. BET analysis. The Brunauer–Emmett–Teller (BET) analysis showed a drastic decrease in the surface area from 132.375 m^2 g^{-1} of AHF to 38.065 m^2 g^{-1} for AHFC whereas it decreased slightly to 111.125 m^2 g^{-1} for AHFT. This could be due to the disintegration of the wall structure at the high temperature and pressure conditions used in hydrothermal carbonisation or due to the modification of the surface chemistry of the hydrochar leading to less affinity for N$_2$ adsorption.[36] The N$_2$ adsorption desorption curves indicated type IV adsorption typical of porous materials (Fig. S1 in ESI†). The pore
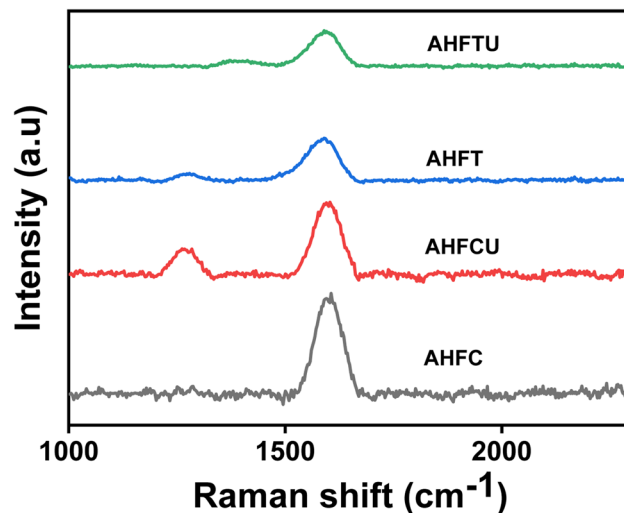

Fig. 5 Raman spectra of AHFC, AHFCU, AHFT and AHFTU.

Table 2 BET parameters of AHF, AHFC and AHFT

BET parameters	AHF	AHFC	AHFT
Total pore volume [cm^3 g^{-1}]	0.014	0.024	0.016
Pore diameter [nm]	1.530	3.415	3.067
Surface area [m^2 g^{-1}]	132.375	38.065	111.125

volume and pore size increased on carbonisation and both AHFC and AHFT showed mesoporous structure with numerous pores on the surface (Table 2). From the data it could be interpreted that AHFC had better porosity than AHFT resulting in its better adsorption efficiency.

3.2.4. XPS analysis. The high resolution C1s XPS spectra of the adsorbents before and after adsorption uranium are shown in Fig. 6a and b. The peaks at 284.74 eV, 286.47 eV and 288.34 eV correspond to C=C, C–O and C=O in AHFC whereas in AHFCU the corresponding peaks were obtained at 284.81 eV, 286.49 eV and 288.34 eV. In AHFT, the C1s peaks were obtained at
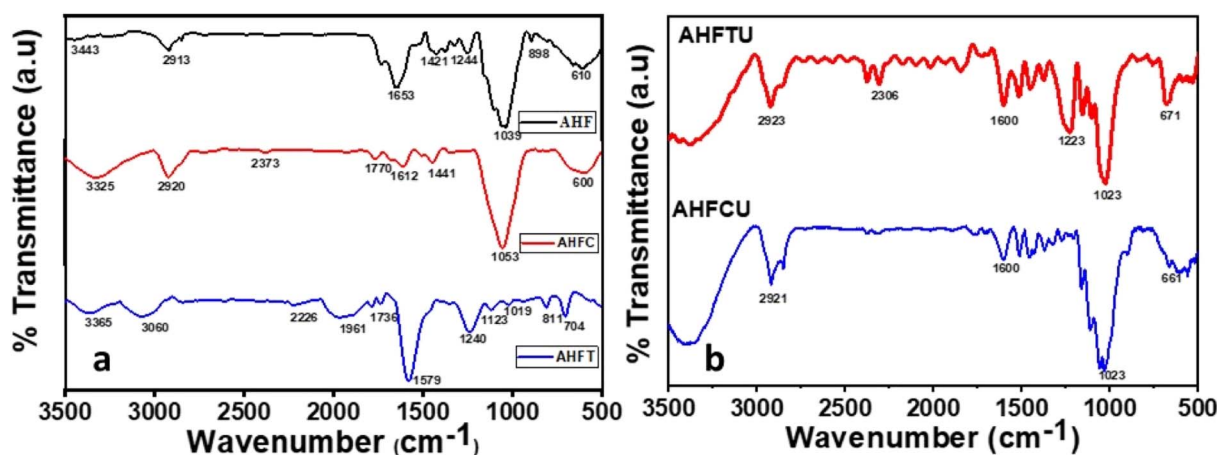

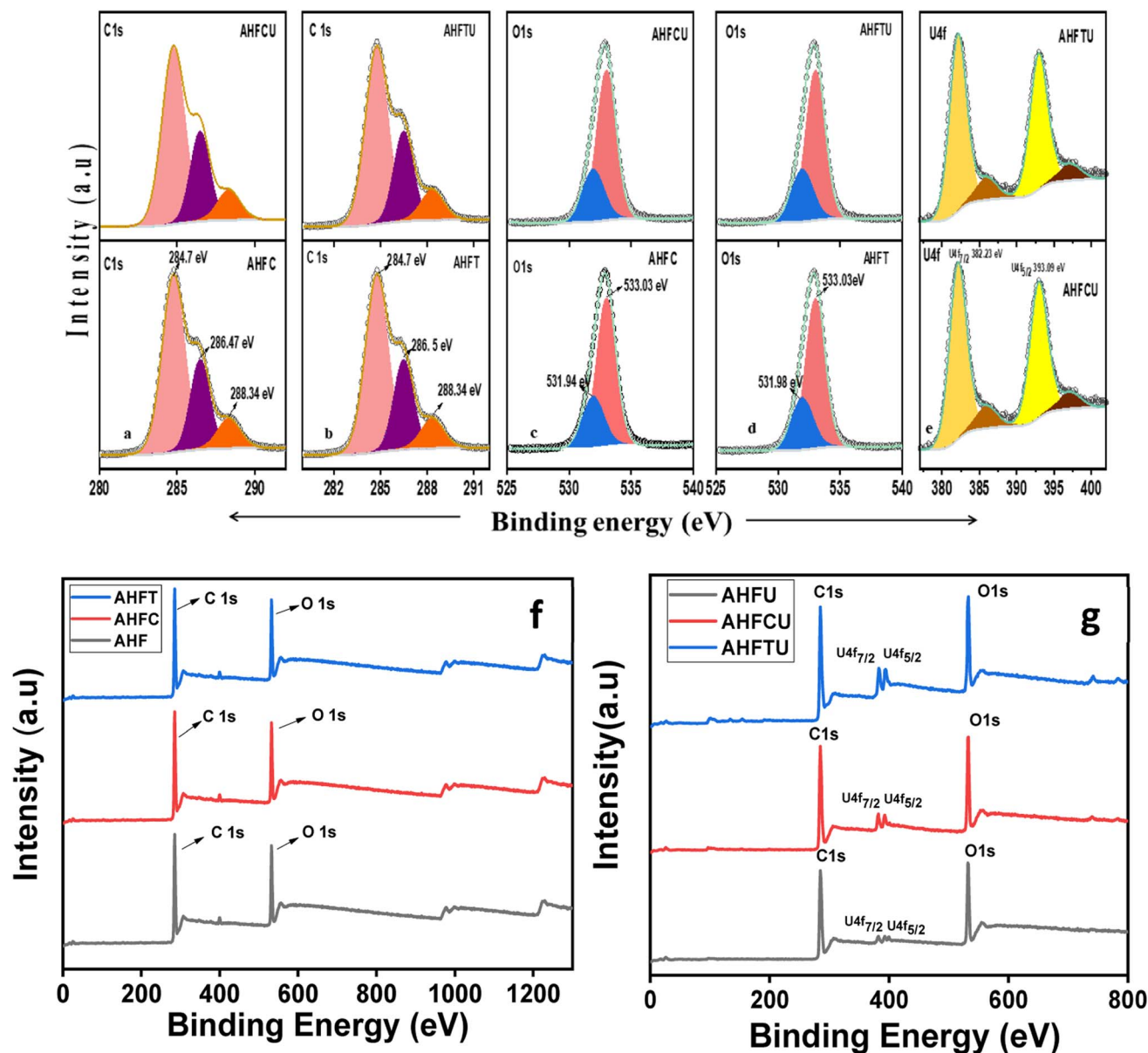**Fig. 4** FT-IR Spectra of (a) AHF, AHFC and AHFT (b) AHFCU and AHFTU.

Fig. 6 High resolution XPS spectra of (a) C1s of AHFC and AHFCU (b) C1s of AHFT and AHFTU (c) O1s of AHFC and AHFCU (d) O1s of AHFC and AHFCU (d) O1s of AHFT and AHFTU (e) U4f of AHFCU and AHFTU (f) XPS survey scan spectra of AHF, AHFC, AHFT and AHFTU (g) XPS survey scan spectra of AHFU, AHFCU, and AHFTU.

284.76 eV (C=C), 286.49 eV (C–O) and 288.34 eV (C=O) while AHFTU showed peaks at 284.81 eV (C=C), 286.52 eV (C–O) and 288.34 eV (C=O).[37] The slight shift in binding energies observed could be attributed to the interaction of the metal ions with the functional groups on the surface of the adsorbents. The O1s spectra (Fig. 6c and d) showed peaks at 533.03 eV (C–O) for both the adsorbents before and after adsorption and at 531.94 eV and 531.98 eV respectively for AHFC and AHFT corresponding to C=O.[38] The survey scan spectra after adsorption showed the presence of uranium on AHFCU and AHFTU (Fig. 6f and g). The two distinct peaks at 382.23 eV and 393.09 eV for $U4f_{7/2}$ and $U4f_{5/2}$ respectively confirmed the presence of uranium in its hexavalent oxidation state.[39] The binding energy

values and the intensities of the C1s and O1s peaks of the adsorbents did not change much after adsorption indicating the adsorption by AHFC and AHFT to be majorly driven by a physicochemical mechanism with diffusion of the adsorbate through the porous layers being the major driving force as compared to the strong covalent bonding interactions.

3.2.5. TGA analysis. The TGA curves (Fig. S2 in ESI†) for the materials indicated AHF to be more thermally labile than AHFC and AHFT decomposing at about 200 °C. AHFT was comparably more stable decomposing gradually above 350 °C while AHFC showed a drastic weight loss at 300 °C indicating the volatilization of the char at this temperature.[40]
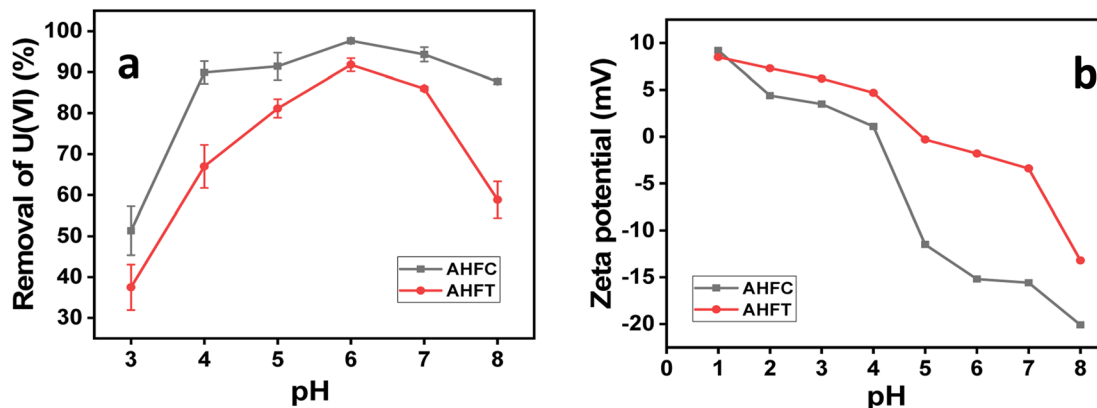
Fig. 7 (a) Effect of pH on adsorption of U(ᴠɪ) by AHFC and AHFT (b) zeta potential in the pH range 1–8 for AHFC and AHFT.

3.3. Batch adsorption of uranium

3.3.1. Effect of pH on adsorption. Adsorption of uranium from aqueous solution is highly pH dependent. The adsorption behavior of AHFC and AHFT were evaluated in the pH range of 3 to 8 and it was found that the adsorption is maximum at pH 6 for both the adsorbents (Fig. 7a). Infact the removal percentage of uranium remained above 90% in the pH range of 5 to 7 for AHFC whereas it increased steadily to reach a maximum at pH 6 for AHFT. Both the adsorbents showed reasonably good adsorption efficiency at near neutral pH and this is crucial in application to ground water contaminated with uranium. The surface zeta potential of both the adsorbents were found to be negative and became increasingly negative with increase in pH suggesting successive deprotonation of the adsorbents (Fig. 7b). This made it convenient for the uranyl species, UO_2^{2+}, UO_2OH^+ and $(UO_2)_2(OH)_2^{2+}$ predominantly present in the pH range below 6.65 to get adsorbed on to the surface through electrostatic interactions.[41] As the pH increases to the alkaline range, different anionic species like $((UO_2)_3(OH)_7)^-$ and $UO_2(OH)_3^-$ are formed due to hydrolysis and also possible complexation with dissolved CO_2 leads to formation of $[(UO_2)_2CO_3(OH)_3]^-$ and $[UO_2(CO_3)_3]^{4-}$ leading to repulsion by the negatively charged adsorbents and hence the decreased adsorption of the metal.[42] The surface zeta potential of AHFC and AHFT was measured in the pH range of 1 to 8. It was found that the zeta potential

became increasingly negative for both the adsorbents with increase in pH of the solution. The negative potential values remained almost constant in the pH range 5 to 7 facilitating easy adsorption of the positively charged uranium species on the surface of the sorbents. Thereafter the potential became more negative but adsorption efficiency decreased as the negatively charged uranium ions at alkaline pH got repelled by the surface. The surface negative charge of AHFC was found to be more negative than that of AHFT at the optimised pH of 6 which is in favour of the better adsorption capacity of AHFC as calculated from isotherm studies.

3.3.2. Adsorption kinetics. Studying the kinetics of the interaction between the adsorbate and the adsorbent is crucial in establishing the mechanism of adsorption.[43] A solution with an initial uranium concentration of 50 mg L^{-1} at pH 6 with an adsorbent dosage of 0.02 g in a sample volume of 0.05 L was used for the kinetic study. The equilibrium was attained in sixty minutes. The data obtained (Fig. 8 and 9) was fitted to pseudo-first order, pseudo-second order and intra-particle diffusion models according to the equations below.

$$\log(q_e - q_t) = \log q_e - (K_1/2.303)t \tag{3}$$

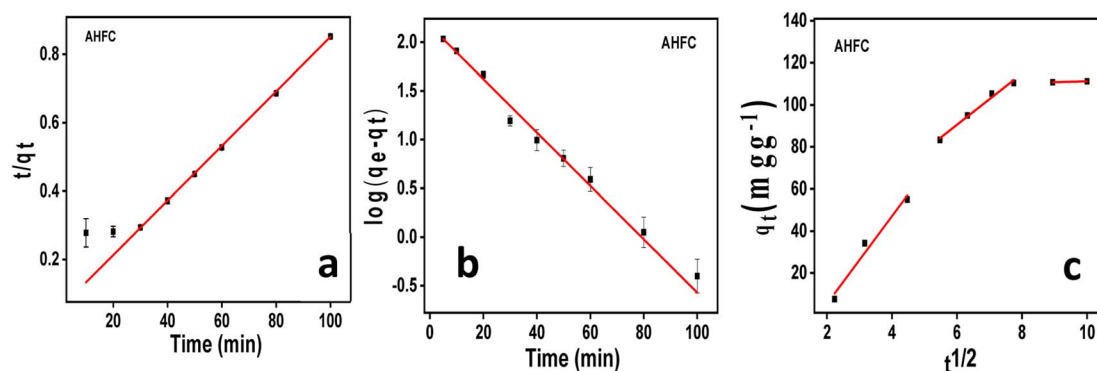$$\frac{t}{q_t} = \frac{t}{q_e} + \frac{1}{K_2 q_e^2} \tag{4}$$

Fig. 8 Adsorption kinetics of U(ᴠɪ) removal by AHFC (a) pseudo-first order, (b) pseudo-second order and (c) intra-particle diffusion model.
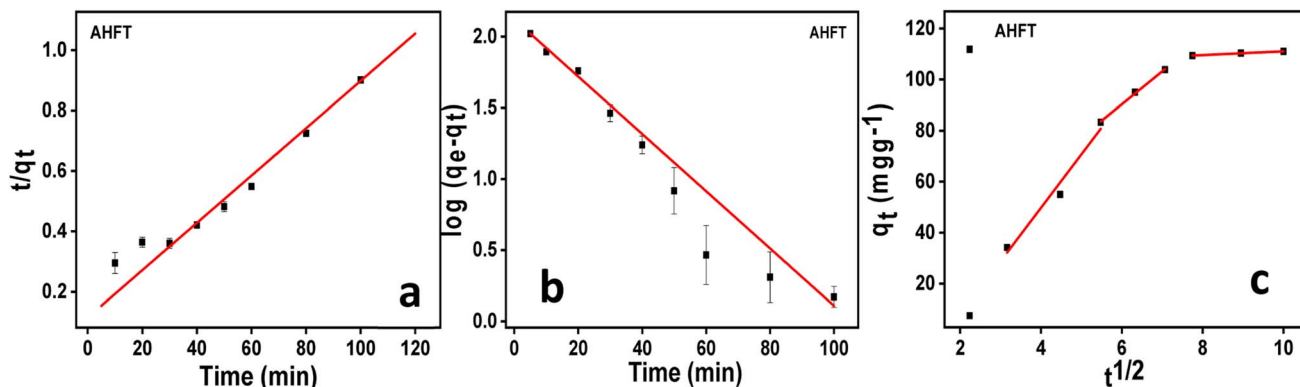

Fig. 9 Adsorption kinetics of U(VI) removal by AHFT (a) pseudo-first order, (b) pseudo-second order and (c) intra-particle diffusion model.

$$q_t = t^{1/2}K_i + C \qquad (5)$$

where K_1 (min^{-1}) and K_2 (g mg^{-1} min^{-1}) are the adsorption rate constants of the pseudo first order and pseudo second order kinetics respectively, t (min) is the adsorption time, q_e (mg g^{-1}) and q_t (mg g^{-1}) are the adsorption quantities at equilibrium and at time t respectively. K_i is the intra-particle diffusion rate constant (mg g^{-1} min$^{-1/2}$) and C is the intercept that gives information on the thickness of the boundary layer.

The adsorption of uranium by both AHFC and AHFT followed pseudo-second order kinetics as indicated by the R^2 values given in Table S1 in ESI.† The removal efficiency steadily increased and reached up to 90% in 50 minutes and the equilibrium was attained at one hour for both the adsorbents. The values obtained for the second order rate coefficients for both the adsorbents were found to be the same indicating similarity in the mechanism of adsorption process. The linearity of intra-particle diffusion plots indicates the adsorption to be
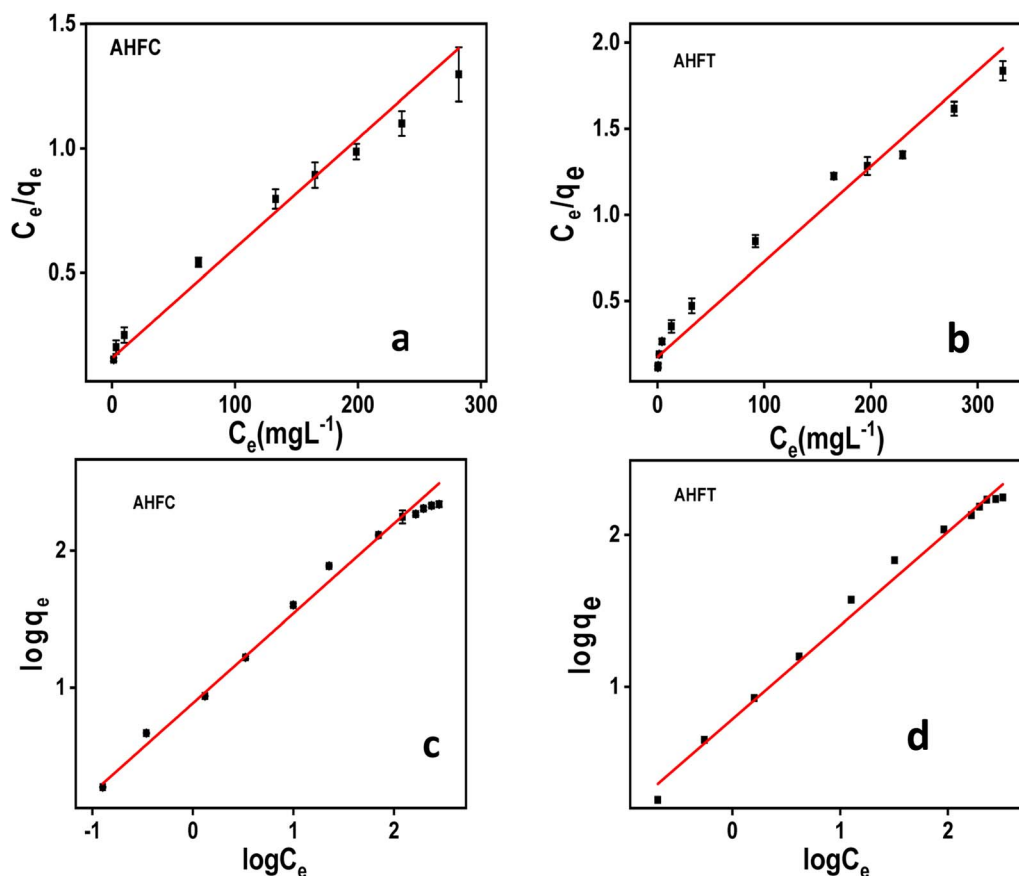

Fig. 10 Adsorption isotherms of uranium on AHFC and AHFT (a) Langmuir isotherm of AHFC (b) Langmuir isotherm of AHFT (c) Freundlich isotherm of AHFC (d) Freundlich isotherm of AHFT.

Table 3 Comparison of adsorption capacity with a few recently reported biochar based adsorbents for remediation of uranium from water

Adsorbent	q_{max} (mg g^{-1})	pH	References
Pyrochar from animal manure	221	4.5	48
HNO$_3$ modified biochar from wheat straw	355	4.5	49
MnO$_2$ modified algal biochar	100	6.0	50
Magnetic water melon rinds biochar	323	4.0	51
Magnetic rice husk biochar	118	7.0	52
Biochar from *Tribulus terrestris* plant biomass	49	6.0	53
Biochar from eucalyptus wood	27.2	5.5	54
Hydrochar from arecanut husk fiber	250	6	This study

a diffusion controlled rate limiting process.[44] The K_i values gradually decreased as adsorption reached saturation whereas the values of C decreased pointing to the rapid mass exchange in the initial phase of adsorption while diffusion through the pores being the driving force near saturation. This observation could be closely correlated to the porous and layered structure of the adsorbents which facilitates the intake of the metal ion.

3.3.3. Adsorption isotherm studies. Batch adsorption experiments were conducted using AHFC and AHFT from 10 mL solution containing 10 mg L^{-1} of uranium with an adsorbent dosage of 10 mg at pH 6. The adsorption data obtained was fitted graphically for varying uranium concentrations to the linear Langmuir and Freundlich isotherm eqn (6) and (7).

$$\frac{C_e}{q_e} = \frac{C_e}{q_{max}} + \frac{1}{q_{max} K_L} \tag{6}$$

where C_e is the equilibrium concentration of uranium in solution (mg L^{-1}), q_e is the amount of U(VI) adsorbed at equilibrium per unit weight of the adsorbent (mg g^{-1}), q_{max} is the maximum adsorption capacity for monolayer coverage (mg g^{-1}) and K_L (L mg^{-1}) is the Langmuir constant which correlates with surface area and pore volume. From the linear Langmuir plot of C_e/q_e against C_e, the slope gives $1/q_{max}$.

$$\log q_e = \log K_F + \frac{1}{n} \log C_e \tag{7}$$

where K_F is the adsorption capacity (mg$^{1-1/n}$ g^{-1} L$^{1/n}$) and n represents the Freundlich coefficient. K_F, q_e and n values are calculated through linear regression analysis. The adsorption data (Fig. 10) fitted well with both Langmuir and Freundlich models and the maximum adsorption capacities calculated for AHFC and AHFT were found to be 250 mg g^{-1} and 200 mg g^{-1} respectively. From the R^2 values obtained it is evident that the adsorption follows Freundlich model suggesting the adsorption process to be multilayer and heterogenous in nature which could be attributed to the porosity and the graphitic layered structure of the carbonaceous adsorbents (Table S2 in ESI†). The separation factor R_L given by eqn (8) indicates the nature of adsorption with $R_L = 1$ indicating linear, $R_L = 0$ as irreversible, $R_L > 1$ unfavorable and $0 < R_L < 1$ as favourable.[45] The calculated R_L

value for an initial uranium concentration of 10 mg L^{-1} is 0.797 and 0.777 respectively for AHFC and AHFT which confirms the favourable nature of adsorption on both AHFC and AHFT.

$$R_L = \frac{1}{1 + C_o K_L} \tag{8}$$

The values of n obtained from Freundlich plot are 1.527 and 1.620 respectively for AHFC and AHFT, both of which fall in the range 1 to 10 indicating the effective adsorption of uranium on the adsorbents. Comparatively AHFC shows better adsorption capacity than AHFT which could be attributed to the functional groups present and the better porosity of the hydrochar.

A comparison of the adsorption capacities reported for different biochars are compiled in Table 3. It is evident that among the unmodified biochars, the adsorbents reported in this work show much better adsorption capacity at near neutral pH and are promising materials for removal of uranium from water.

3.3.4. Thermodynamic study. The effect of temperature on the adsorption of uranium by AHFC and AHFT was evaluated. The diffusion rate of the metal species through the pores of the sorbents vary with temperature and hence the adsorption capacities.[46]

The linear form of van't Hoff equations plotted using the adsorption data at different temperatures were used to calculate the thermodynamic state functions $\Delta H°$ (kJ mol^{-1}), $\Delta G°$ (kJ mol^{-1}) and $\Delta S°$ (J mol^{-1} K^{-1}).

$$\ln K_{eq} = \frac{-\Delta H°}{R}\left(\frac{1}{T}\right) + \frac{\Delta S°}{R} \tag{9}$$

$$\Delta G° = -RT \ln K_{eq} \tag{10}$$

where K_{eq} is the equilibrium constant obtained from the ratio of concentration of uranium ions on the adsorbent surface to that in the solution phase. The enthalpy and entropy changes during
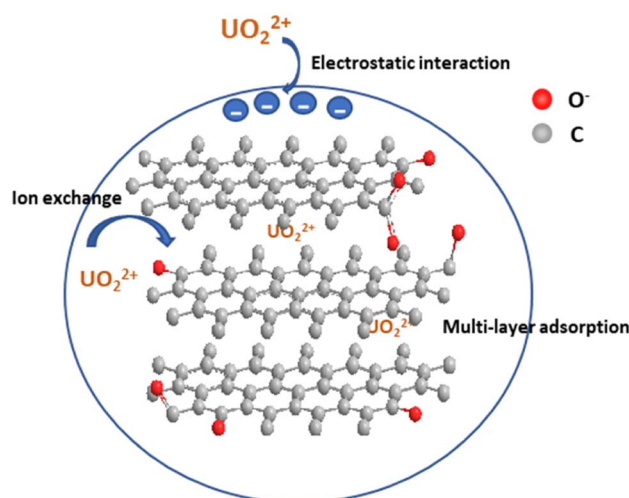

Fig. 11 Schematic representation of adsorption of uranium on adsorbents.
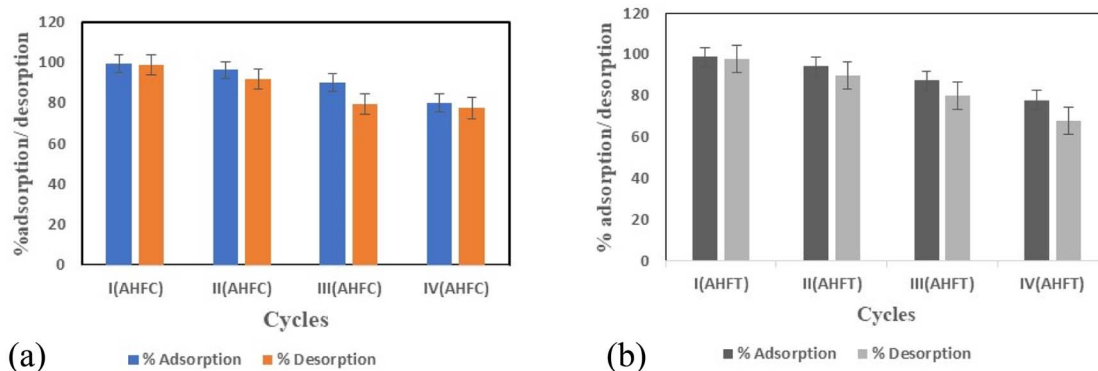
Fig. 12 Reusability of (a) AHFC and (b) AHFT for U(VI) adsorption.

adsorption were calculated using the slope and intercept values obtained from ln K_{eq} against $1/T$ plot (Fig. S3 ESI†). The negative $\Delta G°$ values obtained at different temperatures for both the adsorbents indicated the spontaneity of the adsorption process. The adsorption process is predominantly controlled by physisorption for both AHFC and AHFT as is indicated by the negative enthalpy change values (Table S3 in ESI†).

3.4. Mechanism of interaction between uranium and the adsorbents

The data obtained from the detailed characterization of the adsorbents before and after adsorption and other parameters indicate that the adsorption by AHFC and AHFT is physicochemical in nature and is an energetically favorable process. The oxophilicity of uranyl ions and the presence of oxygen containing functional groups like C=O and C–O on the adsorbents helped the binding of the ions on the surface of the adsorbents. The appearance of new peaks at 661 cm^{-1} and 671 cm^{-1} AHFCU and AHFTU corresponding to U–O bonding interaction suggested the binding of uranium on to the

adsorbents. As indicated by the BET and SEM-EDAX data, the nature of the adsorbents in terms of porosity, surface area and good pore volume could be the major driving force for the effective adsorption of the metal ions. Also the surface negative charge of the adsorbents as indicated by the zeta potential values facilitated the electrostatic interactions between the positively charged ions and the adsorbents. At the optimized pH of 6, the metal ion majorly exists in UO_2^{2+}, UO_2OH^+ and $(UO_2)_2(OH)_2^{2+}$ forms which assist the electrostatic interactions. The isotherm studies showed that the adsorption adhered more with Freundlich model for both the adsorbents suggesting a multilayer process. This along with the inference from Raman spectra on the graphitic layered arrangement of carbon atoms contributed to the diffusion of adsorbate into the adsorbent. Overall, the adsorption by AHFC and AHFT is favoured by the synergistic influence of these factors (Fig. 11).

3.5. Desorption and regeneration of the adsorbents

The sustainability and utility of a material as an adsorbent depends greatly on its regeneration capacity and reusability.
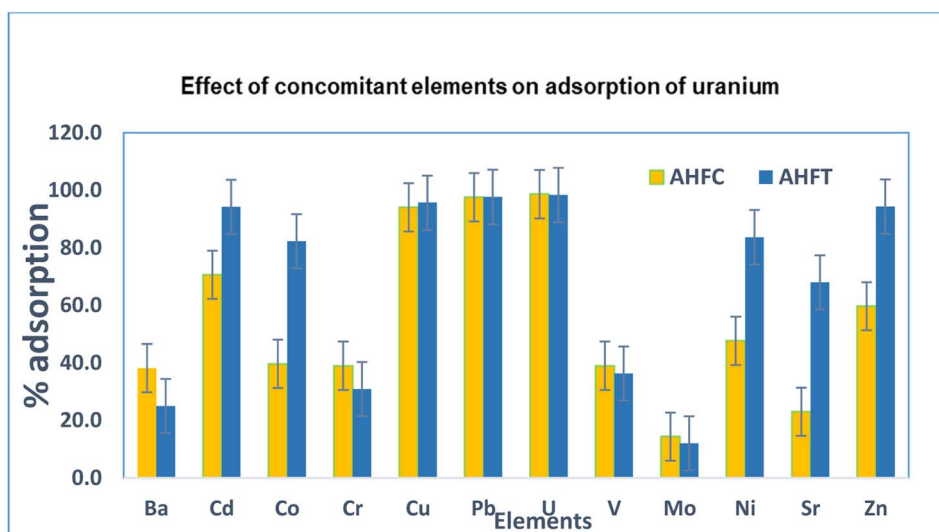

Fig. 13 Selectivity of AHFC and AHFT to uranium over other ions at initial concentrations of 1.0 mg L^{-1}.

Desorption experiments were performed with both the adsorbents using 0.5 M HNO_3 solution and the results are tabulated in Fig. 12. A nearly hundred percent desorption (99.9%) of the adsorbed uranium was observed for AHFCU and that for AHFTU was about 99% after the first cycle of regeneration. The subsequent use of the regenerated adsorbents for adsorption–desorption cycles showed an adsorption efficiency of 80% and 78% respectively for AHFC and AHFT up to 4 cycles. Hence, it is envisaged that these ecofriendly materials could be effectively used for remediation of uranium from aqueous systems.

3.6. Selectivity of the adsorbents to uranium

The selectivity of the adsorbents to uranium was evaluated in the presence of other divalent metal ions (Ba, Cd, Co, Cr, Cu, Mo, Ni, Pb, Sr, V and Zn) from 20 mL of 1.0 mg L^{-1} metal ion solution using 20 mg of the adsorbents at pH 6 (Fig. 13). The efficacy of removal was found to follow the order Pb > U > Cu > Cd > Zn > Ni > Co > Cr > Ba > V > Sr > Mo for AHFC and Pb > Cu > Cd > U > Zn > Ba > Ni > Co > Sr > V > Cr > Mo for AHFT.

In the case of AHFC, only lead was slightly more adsorbed (99.7%) than uranium (98.9%) while all other metal ions were adsorbed to a lesser extend confirming the high selectivity of the adsorbent towards uranium. AHFT also showed very good selectivity over most of the metal ions which have a probability of coexisting with uranium in aqueous environments. The selectivity towards adsorption of uranium was significantly higher than that for vanadium which is usually found along with uranium in sea water indicating the usefulness of the adsorbents for decontamination of uranium from seawater.[47] Among the concomitant ions, molybdenum was adsorbed to the least by both the adsorbents. The study clearly indicated the good adsorption efficiency of the sorbents not just towards uranium but for other common heavy metal pollutants in water like Pb, Cd, Cu *etc* and hence could prove versatile in environmental applications.

3.7. Application to groundwater samples

Both AHFC and AHFT were used for adsorptive removal of uranium from ground water samples collected from different borewells in and around Hyderabad and one sample from Bhatinda, Punjab, India. Each of these environmental samples were doped with uranium (1000 ng mL^{-1}) much above the permissible limit for drinking water. The Table 4 compiles the data obtained from analysis of various physico-chemical parameters of the water samples. The pH of all the samples lied between 7 to 8. Under this pH conditions uranium is known to be present as its bicarbonate complex. Soluble Na and K ions generally do not affect the adsorption efficiencies. AHFC showed superior adsorptive capacity compared to AHFT for all the samples. The adsorption was influenced by the varying concentrations of the ions present in the samples. The analysis showed a removal efficiency of around 88% for AHFC and around 83% for AHFT in presence of HCO_3^- (av. 400 ppm); F$^-$ (av. 2 ppm); SO_4^{2-} (av. 200 ppm) and other complexing ions.

Table 4 Spike recovery of U(VI) in ground water samples and the multi-ions present in those samples by AHFC and AHFT

Sample no.	U in sample (ng mL^{-1})	U Spiked (ng mL^{-1})	U adsorbed (%) AHFC	U adsorbed (%) AHFT	pH	Conductivity (mS cm^{-1})	Na$^+$ (µg mL^{-1})	K$^+$ (µg mL^{-1})	Ca^{2+} (µg mL^{-1})	Mg^{2+} (µg mL^{-1})	Cl$^-$ (µg mL^{-1})	F$^-$ (µg mL^{-1})	HCO$_3^-$ (µg mL^{-1})	SO$_4^{2-}$ (µg mL^{-1})	NO$_3^-$
GW 1	42	1000	90	86	7.3	1.4	120	5	180	30	190	1.6	411	117	122
GW 2	38	1000	85	80	7.0	1.3	144	3	114	37	134	1.6	482	113	38
GW 3	88	1000	80	75	7.6	2.2	452	9	60	66	210	2.4	572	582	6
GW 4	13	1000	93	88	7.8	1.3	129	2	108	19	167	1.0	213	100	15
GW 5	2	1000	90	87	7.9	2.0	320	3	70	20	202	1.4	331	250	10
GW 6	7	1000	91	86	7.2	1.8	228	2	78	20	163	1.3	294	100	22

4. Conclusions

Two novel ecofriendly adsorbents (AHFC and AHFT) for uranium remediation from aqueous systems were synthesized through simple hydrothermal carbonization in aqueous medium and pyrolytic pathways from arecanut husk fiber, an agricultural waste material. A comprehensive characterization of the adsorbents before and after the adsorption indicated the porosity, surface area, layered structure and functional groups on the adsorbents attributed to the binding of the metal ion. Maximum adsorption capacities of 250 mg g^{-1} and 200 mg g^{-1} were obtained for AHFC and AHFT respectively at an optimized pH of 6. The results from selectivity studies and the application to ground water samples indicate the possibility of these low cost, non-toxic materials to be upgraded to filter materials by appropriate modifications for the removal of uranium from contaminated water. The highlight of the work is the cradle to cradle approach adopted in alignment with the GOAL-6 (clean water and sanitation) of UNSDGs – 2030.

Author contributions

Rajesh was instrumental in the conceptualization of the study. Dhanya performed all the experimental studies, characterizations, the interpretation of data and the overall presentation of the manuscript. The authors concur towards their respective contributions.

Conflicts of interest

The authors declare no conflict of interest.

Acknowledgements

References

1 T. P. Gandhi, P. V. Sampath and S. M. Maliekkal, *Sci. Total Environ.*, 2022, **825**, 153947.

2 V. Balarama, A. Rani and D. P. S. Rathore, *GeoGeo*, 2022, **1**, 100043.

3 *Report by CGWB*, Department of Water Resources, Government of India, 2020.

4 S. Banerjee, A. Kundu and P. Dhak, *J. Radioanal. Nucl. Chem.*, 2022, **331**, 2409–2435.

5 J. Shen and A. Schäfer, *Chemosphere*, 2014, **117**, 679–691.

6 R. Foster, J. Amphlett, K.-W. Kim, T. Kerry, K. Lee and C. Sharrad, *J. Ind. Eng. Chem.*, 2019, **81**, 144–152.

7 Y. Ruan, H. Zhang, Z. Yu, Z. Diao, G. Song, M. Su and L. Kong, *J. Hazard. Mater.*, 2022, **424**, 127119.

8 F. Ma, Y. Gui, P. Liu, Y. Xue and W. Song, *Chem. Eng. J.*, 2020, **390**, 124597.

9 Y. Xie, Z. Zhang, Z. Dong, R. Zhou, X. Cao, Y. Liu and X. Wang, *Environ. Nanotechnol. Monit. Manag.*, 2021, **16**, 100510.

10 V. Dhanya, B. Arunraj and N. Rajesh, *RSC Adv.*, 2022, **12**, 13511.

11 S. Verma and Ki-H. Kim, *Environ. Int.*, 2022, **158**, 106944.

12 W. R. Cui, F. F. Li, R. H. Xu, C. R. Zhang, X. R. Chen, R. H. Yan and J. D. Qiu, *Angew. Chem., Int. Ed.*, 2020, **59**, 17684–17690.

13 H. Liu, T. Fu and Y. Mao, *ACS Omega*, 2022, **7**, 14430–14456.

14 F. Wang, Y. Liao and L. Xia, *J. Solid State Chem.*, 2021, **303**, 122511.

15 L. Ding, B. Chen, Y. Wang and Y. Zhang, *Process Saf. Environ. Prot.*, 2022, **168**, 1049–1057.

16 T. Tatarchuk, A. Shyichuk, I. Mironyuk and M. Naushad, *J. Mol. Liq.*, 2019, **293**, 111563.

17 S. Kumar, V. A. Loganathan, R. B. Gupta and M. O. Barnett, *J. Environ. Manage.*, 2011, **92**, 2504–2512.

18 X. Li, Z. Liu and M. Huang, *J. Radioanal. Nucl. Chem.*, 2022, **331**, 3043–3075.

19 U. K. Banala, N. P. I. Das and S. R. Toleti, *Environ. Technol. Innov.*, 2020, **21**, 101254.

20 T. Ye, B. Huang, Y. Wang, L. Zhou and Z. Liu, *Colloids Surf, A Physicochem Eng Asp*, 2020, **606**, 125480.

21 Z. Chen, R. Zheng, W. Wei, W. Wei, W. Zou, J. Li, B. J. Ni and H. Chen, *Resour. Conserv. Recycl.*, 2022, **178**, 106037.

22 Z. Chen, W. Wei, B. J. Ni and H. Chen, *Environ. Funct. Mater.*, 2022, **1**, 34–48.

23 Z. Chen, W. Wei, H. Chen and B. J. Ni, *Eco-Environ. Health*, 2022, **1**, 86–104.

24 S. Shyam, J. Arun, K. P. Gopinath, G. Ribhu, M. Ashish and S. Ajay, *Chemosphere*, 2022, **86**, 131490.

25 Y. Dai, N. Zhang, C. Xing, Q. Cui and Q. Sun, *Chemosphere*, 2019, **223**, 12–27.

26 Z. Liu, Z. Xu, L. Xu, F. Buyong, T. C. Chay, Z. Li, Y. Cai, B. Hu, Y. Zhu and X. Wang, *Carbon res.*, 2022, **1**, 8, DOI: 10.1007/s44246-022-00007-3.

27 W. Ahmed, S. Mehmood, M. Qaswar, S. Ali, Z. H. Khan, H. Ying, D. Y. Chen and A. Núñez-Delgado, *J. Environ. Chem. Eng.*, 2021, **9**, 105104.

28 L. Dong, J. Yang, Y. Mou, G. Sheng, L. Wang, W. Linghu, A. M. Asiri and K. A. Alamry, *J. Radioanal. Nucl. Chem.*, 2017, **314**, 377–386.

29 M. Fan, X. Wang, Q. Song, L. Zhang, B. Ren and X. Yang, *J. Radioanal. Nucl. Chem.*, 2021, **330**, 589–602.

30 L. P. Padhye, E. R. Bandala, B. Wijesiri, A. Goonetilleke and N. Bolan, *Front. chem. eng.*, 2022, **4**, 867228.

31 W. Zheng, X. Li, F. Wang, Q. Yang, P. Deng and G. Zeng, *J. Hazard. Mater.*, 2008, **157**, 490–495.

32 S. Ramesh, P. Sundararaju, K. S. P. Banu, S. Karthikeyan, U. Doraiswamy and K. Soundarapandian, *Environ. Sci. Pollut. Res.*, 2019, **26**, 3751–3761.

33 H. Wikberg, T. Ohra-aho, F. Pileidis and M. M Titirici, *ACS Sustain. Chem. Eng.*, 2015, **3**, 2737–2745.

34 B. Singh, S. Mahajan, H. N. Sheikh and B. L. Kalsotra, *J. Saudi Chem. Soc.*, 2014, **18**, 494–501.

35 J. B. Wu, M. L. Lin, X. Cong, H. N. Liu and P. H. Tan, *Chem. Soc. Rev.*, 2018, **47**, 1822–1873.

36 Y. Zhou, B. Gao, A. R. Zimmerman, J. Fang, Y. Sun and X. Cao, *Chem. Eng. J.*, 2013, **231**, 512–518.

37 X. Chen, X. Wang and D. Fang, *Fuller. Nanotub. Carbon Nanostructures*, 2020, **28**, 1048–1058.

38 Y. Sun, B. Zeng, Y. Da, X. Liang, L. Zhang, R. Ahmad and X. Su, *J. Colloid Interface Sci.*, 2022, **614**, 547–555.

39 E. S. Ilton and P. S. Bagus, *Surf. Interface Anal.*, 2011, **43**, 1549–1560.

40 J. Zhao, W. Xiuwen, J. Hu, Q. Liu, D. Shen and R. Xiao, *Polym. Degrad. Stab.*, 2014, **108**, 133–138.

41 A. Jana, A. Unni, S. S. Ravuru, A. Das, D. Das, S. Biswas and H. S. S. De, *Chem. Eng. J.*, 2022, **428**, 131180.

42 Z. Ahmad, Y. Li, J. Yang, N. Geng, Y. Fan, X. Gou, Q. Sun and J. Chen, *J. Hazard. Mater.*, 2022, **425**, 127995.

43 S. Gupta and K. G. Bhattacharyya, *Adv. Colloid Interface Sci.*, 2011, **162**, 39–58.

44 A. A. Aryee, F. M. Mpatani, A. N. Kani, E. Dovi, R. Han, Z. Li and L. Qu, *Environ. Sci. Pollut. Res.*, 2020, **27**, 40316–40330.

45 M. A. Al-Ghouti and D. A. Da'ana, *J. Hazard. Mater.*, 2020, **393**, 122383.

46 D. Shao, Y. Li, X. Wang, S. Hu, J. Wen, J. Xiong, A. M. Asiri and H. M. Marwani, *ACS Omega*, 2016, **2**, 3267–3275.

47 Q. Gao, J. Hu, R. Li, Z. Xing, L. Xu, M. Wang and G. Wu, *Radiat. Phys. Chem.*, 2016, **122**, 1–8.

48 L. Han, E. Zhang, Y. Yang, K. Sun and L. Fang, *J. Clean. Prod.*, 2020, **264**, 121542.

49 J. Jin, S. Li, X. Peng, W. Liu, C. Zhang, Y. Yang, L. Han, Z. Du, K. Sun and X. Wang, *Bioresour. Technol.*, 2018, **256**, 247–253.

50 B. Wang, J. Zheng, Y. Li, A. Zaidi, Y. Hu and B. Hu, *J. Environ. Chem. Eng.*, 2021, **9**, 105625.

51 L. P. Lingamdinne, J.-S. Choi, G. K. R. Angaru, R. R. Karri, J.-K. Yang, Y.-Y. Chang and J. R. Koduru, *Chemosphere*, 2022, **86**, 131776.

52 S. Wang, W. Guo, F. Gao, Y. Wang and Y. Gao, *RSC Adv.*, 2018, **8**, 13205–13217.

53 W. Ahmed, S. Mehmood, A. Núñez-Delgado, M. Qaswar, S. Ali, H. Ying and D.-Y. Chen, *Sci. Total Environ.*, 2021, **780**, 146617.

54 V. Mishra, M. K. Sureshkumar, N. Gupta and C. P. Kaushik, *Water, Air, Soil Pollut.*, 2017, **228**, 309.